Skeletal Radiology (2019) 48:721–728
https://doi.org/10.1007/s00256-018-3116-0

SCIENTIFIC ARTICLE

Susceptibility-weighted MR imaging to improve the specificity of erosion detection: a prospective feasibility study in hand arthritis

Sevtap Tugce Ulas[1] · Torsten Diekhoff[1,2] · Kay Geert Armin Hermann[1] · Denis Poddubnyy[3] · Bernd Hamm[1] · Marcus Richard Makowski[1]

Received: 10 September 2018 / Revised: 4 November 2018 / Accepted: 12 November 2018 / Published online: 18 December 2018

Abstract

Objective To evaluate the diagnostic potential of susceptibility-weighted imaging (SWI) for the detection of erosions of the hand, compared to T1-weighted (T1w) magnetic resonance imaging (MRI). Computed tomography (CT) was used as a reference standard.

Materials and methods We prospectively investigated 37 patients with suspected arthritic activity of the hand. All patients underwent T1w, SWI, and CT on the same day. Patients were randomized to MRI or CT first. CT, T1w, SWI, and T1w/SWI were scored for erosions according to OMERACT RAMRIS guidelines. Specificity, sensitivity, and diagnostic accuracy were separately calculated for T1w, SWI, and T1w/SWI on a per-patient and per-bone basis using CT as reference. The one-tailed McNemar test was performed to test the number of erosion-positive patients in T1w, SWI, and T1w/SWI for non-inferiority. Measured erosion sizes were compared using Pearson's test.

Results CT was positive for erosions in 16 patients and 55 bones. SWI and T1w/SWI had superior diagnostic accuracy (91.2 and 93.8%) compared to T1w (87.8%) driven by a higher specificity (93.8 and 96.5%) compared to T1w (88.8%). On the patient level, SWI and T1w/SWI showed non-inferiority ($p = 0.11$ and $p = 0.38$) but not T1w alone ($p < 0.0001$). The lesion size on CT correlated better with SWI (Pearson's $r = 0.92$) compared to T1w ($r = 0.69$).

Conclusions Adding SWI to a standard MRI protocol has the potential to improve erosion detection in hands by increasing specificity. SWI depicts bony erosions more accurately compared to standard MRI techniques.

Keywords Magnetic resonance imaging · Computed tomography · Erosive arthropathy · Rheumatoid arthritis

Introduction

Erosions are the hallmark of arthritis and their timely detection is of great importance for optimal therapeutic management and the patient's prognosis [1, 2]. Magnetic resonance imaging (MRI) has been shown to be superior to conventional radiography in the detection of erosions [3–5]. For this purpose, the use of T1-weighted sequences (T1w) is recommended by the Outcome Measurement in Rheumatology (OMERACT) guidelines [6]. However, due to the high signal of fatty bone marrow, T1w allows only indirect depiction of cortical bone [7, 8]. This can result in low specificity and limit the visualization and delineation of erosions on T1w images [9, 10].

Susceptibility-weighted imaging (SWI) is a novel gradient-echo imaging sequence that is currently mainly applied in neuroradiology [11–13]. Exploiting a novel contrast in MRI, SWI enables the characterization of tissues in the body based on their different magnetic susceptibility properties [13, 14]. The resulting changes in phase reconstruction allow the identification of specific tissue properties that are concealed to traditional T1w and T2 weighting [15]. Substances with diamagnetic properties cause a negative phase shift and are, therefore, detected by SWI [15]. One such substance is

Electronic supplementary material The online version of this article (https://doi.org/10.1007/s00256-018-3116-0) contains supplementary material, which is available to authorized users.

✉ Torsten Diekhoff
torsten.diekhoff@charite.de

[1] Department of Radiology, Charité - Universitätsmedizin Berlin, Campus Mitte, Humboldt-Universität zu Berlin, Freie Universität Berlin, Berlin, Germany

[2] Department of Radiology (CCM), Charité – Universitätsmedizin Berlin, Charitéplatz 1, 10117 Berlin, Germany

[3] Department of Rheumatology, Charité - Universitätsmedizin Berlin, Campus Benjamin Franklin, Humboldt-Universität zu Berlin, Freie Universität Berlin, Berlin, Germany

calcium, and, because it is a main component of bone, its effect on the local magnetic field is of particular interest [13]. As a result, destructions or a decrease in the density of calcium-containing bone substance can be detected [16]. SWI therefore has the potential of directly visualizing and assessing cortical and trabecular bone [17]. A recent case report has shown SWI to improve the MR-based differentiation of cortical and trabecular bone compared to T1w [18]. Therefore, SWI may be a useful additional pulse sequence to improve the specificity of conventional MRI for detecting bony changes.

The aim of our study was to assess the feasibility of SWI for the detection of erosions of the hand compared with T1w MR imaging. Computed tomography (CT) was used as standard of reference.

Materials and methods

Subjects

We prospectively included 37 consecutive patients presenting with arthritic activity of the wrist and finger joints to our hospital's rheumatology outpatient center from September 2016 to October 2017. Patients were only included if initial clinical and laboratory findings were concordant with the diagnosis of rheumatoid arthritis. Patients were enrolled regardless of their symptom duration, severity, or current treatment. Exclusion criteria were age under 50, contraindications to MRI, for example pacemaker, cochlear implants, and claustrophobia. The final diagnosis was made by experienced rheumatologists of the local rheumatology department based on established ACR/EULAR diagnostic criteria [19] and the results of the imaging.

The study was approved by the local ethics committee and the Federal Office for Radiation Protection (Z 5-22462/2 – 2016-008), and all patients gave informed consent before study inclusion.

Imaging procedure

All patients underwent MRI and CT of the clinically dominant hand on the same day and were randomized to MRI or CT first. MRI was performed on a 1.5-Tesla scanner (Siemens Magnetom Avanto; Siemens Healthcare; Erlangen, Germany) using a standard clinical protocol, which included SWI and a T1w spin echo sequence in the coronal plane. The sequence parameters for SWI were as follows: slice thickness, 0.8 mm; repetition time (TR), 49 ms; echo time (TE), 20 ms; 15° flip angle (FA); matrix resolution, 192 × 192; field of view (FOV) read, 160 mm; FOV phase, 100%; slice gap, 20%; distance factor, 20%; phase-encoding direction, right to left; 100% phase oversampling; 100% phase resolution; no phase partial Fourier; and no fat or water suppression. SWI was acquired using flow compensation. The acquisition time for SWI was 5:03 min. After acquisition, magnitude and phase images were reconstructed automatically. The T1w sequences were acquired with the following parameters: slice thickness, 3.0 mm; TR, 401 ms; TE, 21 ms; 90° FA; matrix resolution, 512 × 512; FOV read, 160 mm; FOV phase, 100%; slice gap, 10%; distance factor, 10%; phase-encoding direction, right to left; 0% phase oversampling; 100% phase resolution; no phase partial Fourier; no fat or water suppression; and no flow compensation. The duration of the T1w acquisition was 3:29 min. A small flexible four-channel coil (Siemens Healthcare; Erlangen, Germany) was used. CT of the same hand was performed on a 320-row scanner (Canon Aquilion ONE Vision; Canon Medical Systems; Otawara, Japan) without table movement using an ultra-low-dose protocol with a tube voltage of 80 kVp and a tube current of 30 mAs. The CT datasets were reconstructed with a bone kernel and 0.5-mm slice thickness in the coronal plane. All scans were performed in prone and so-called superman position.

Image reading

All images were anonymized separately for SWI, T1w, and CT using Horos (The Horos Project, Version 3.0, Purview, Maryland, USA). The SWI magnitude image was inverted to simulate the impression of a CT scan. The images were scored separately for SWI, T1w, and CT by three readers in consensus. The readers had different years of experience in musculoskeletal imaging: reader 1, a senior radiologist with 10 years, reader 2, a specialist in radiology with 9 years, and reader 3, a medical research student with 1 year of experience in musculoskeletal imaging. The readers were trained and calibrated on a set of test cases and blinded to clinical data and other imaging findings. In a second step, a combined scoring of SWI and T1w images was conducted (T1w/SWI) to assess the additional value of SWI to a standard protocol. All scorings were performed using the OMERACT Rheumatoid Arthritis Magnetic Resonance Imaging Score (RAMRIS) for erosions assigning scores of 0 to 10 separately for the metacarpal bases, carpal bones, distal radius and ulna, as well as the metacarpal head and phalangeal bases II-V [6, 20]. Thereafter, reader 3 assessed the diameter of the surface and the depth of the 31 largest erosions for CT, T1w, and SWI.

Statistical analysis

Statistical analysis was performed using GraphPad Prism (Version 7 for MacOS, GraphPad Software, La Jolla, CA, USA). The scoring results were dichotomized and summarized. Erosions detected in CT served as reference. On the patient level, patients with one or more erosions detected were categorized as erosion-positive irrespective of number and

size. The number of erosion-positive patients in T1w, SWI, and T1w/SWI were compared to CT using a one-tailed McNemar test (to test for non-inferiority). False-positive and false-negative detections in the different modalities were compared with CT for each final diagnosis. On the bone level, the bones were also dichotomized into erosion-positive and -negative irrespective of their size. Diagnostic accuracy was calculated on the per-patient and per-bone level separately for SWI, T1w, and T1w/SWI. Contingency tables were created to calculate sensitivity, specificity, positive predictive value, and negative predictive value of SWI, T1w, and T1w/SWI on the patient level and bone level using the Wilson/Brown method. Furthermore, sum scores were calculated and the Pearson's r test was performed to assess their correlation. The multiplication product of the diameter and depth served to calculate the correlation of quantitative erosion measurement using the two-tailed Pearson's correlation coefficient.

Results

Subjects

In total, 37 patients (27 women, ten men; mean age 60.1, 50–77 years) with a mean weight of 77.3 kg (SD 14.3), a mean C-reactive protein (CRP) of 18 mg/dl (SD 42.6) and a mean duration of symptoms of 3.9 years (SD 4.84) were included in the study. Anti-citrullinated peptide antibodies were positive in 17 patients and the rheumatoid factor was positive in five patients. According to the imaging findings and the ACR/EULAR criteria [19], 25 of the patients were finally diagnosed with rheumatoid arthritis (RA), three with psoriatic arthritis (PsA), one with undifferentiated arthritis (UA), six with osteoarthritis (OA), and two with calcium pyrophosphate deposition disease (CPPD). A flow chart of study inclusion is presented in Fig. 1. The study population consisted of 14 treatment-naïve patients, three patients treated with NSAID solely and six patients receiving corticosteroid only, seven patients DMARD and seven biologicals.

Imaging procedure

SWI, T1w, and CT were conducted in all patients. In 16 patients, MRI was performed first. The dose-length product was estimated to be 8 mGy*cm, corresponding to an effective dose of < 0.01 mSv.

Image reading and statistical analysis

CT was positive for erosions in 16 patients. SWI was positive in 22 patients, T1w in 33 patients, and T1w/SWI in 16 patients. Using the one-tailed McNemar test, SWI and T1w/SWI showed non-inferiority ($p = 0.11$ and $p = 0.38$), but not T1w alone ($p < 0.0001$). Examples of the imaging findings are presented in Fig. 2. The results of contingency table analysis are presented in Table 1. SWI showed false-positive detection in two patients with seropositive RA, four patients with seronegative RA, one patient with UA, three patients with OA, and one patient with CPPD. False-positive erosions in T1w were detected in three patients with seropositive RA, eight patients with seronegative RA, one patient with UA, three patients with OA, and two patients with CPPD. For combined T1w/SWI, one patient with seropositive RA, two patients with seronegative RA, one patient with UA, and one patient with OA had false-positive erosions. False-negative detection in SWI was identified in two patients with seropositive RA and three patients with seronegative RA. No patient was false negative on T1w. T1w/SWI showed false-negative detection in three patients with seronegative RA, one patient with PsA, and one patient with OA.

A total of 850 of the 851 eligible bone regions were assessed by CT, 849 by T1w, and 649 by SWI and T1w/SWI (Fig. 1). The total sum score was 115 for CT, 104 for SWI, 244 for T1w, and 84 for T1w/SWI. Pearson's r test showed a better correlation of SWI with CT compared to T1w ($r = 0.86$ and $r = 0.76$). However, T1w/SWI improved the correlation of the patient sum scores to 0.90. Further details are shown in Table 1 and Fig. 1. In total, 31 erosions were measured in CT. Two erosions in T1w and three erosions in SWI were not sufficiently depicted. CT correlated better with SWI ($r = 0.92$, $p < 0.0001$) compared to T1w ($r = 0.69$, $p < 0.0001$) (Fig. 3).

Discussion

This is the first study investigating SWI for the detection of erosions of the hand. For validation of the MRI findings, CT was used as standard of reference. On the patient level, our results demonstrate non-inferiority of SWI and the combination of SWI and T1w, whereas T1w alone has significantly poorer specificity. On the level of individual bones, our findings show SWI to improve specificity for erosion detection compared to T1w. However, the combination of T1w and SWI has the highest diagnostic accuracy. The correlation of the OMERACT-RAMRIS sum scores with CT was highest for T1w/SWI, followed by SWI alone. The same was demonstrated for erosion size measurements.

Early and accurate detection of erosions is of major clinical relevance for the differential diagnosis and therapy monitoring in patients with inflammatory joint disorders such as rheumatoid arthritis [21]. Erosions usually occur the course of chronic and ineffectively treated inflammatory joint diseases, such as rheumatoid arthritis. The development of erosions predicts future loss of joint function [22–25] and its prevention is the main goal of any treatment in these patients [26]. When erosive

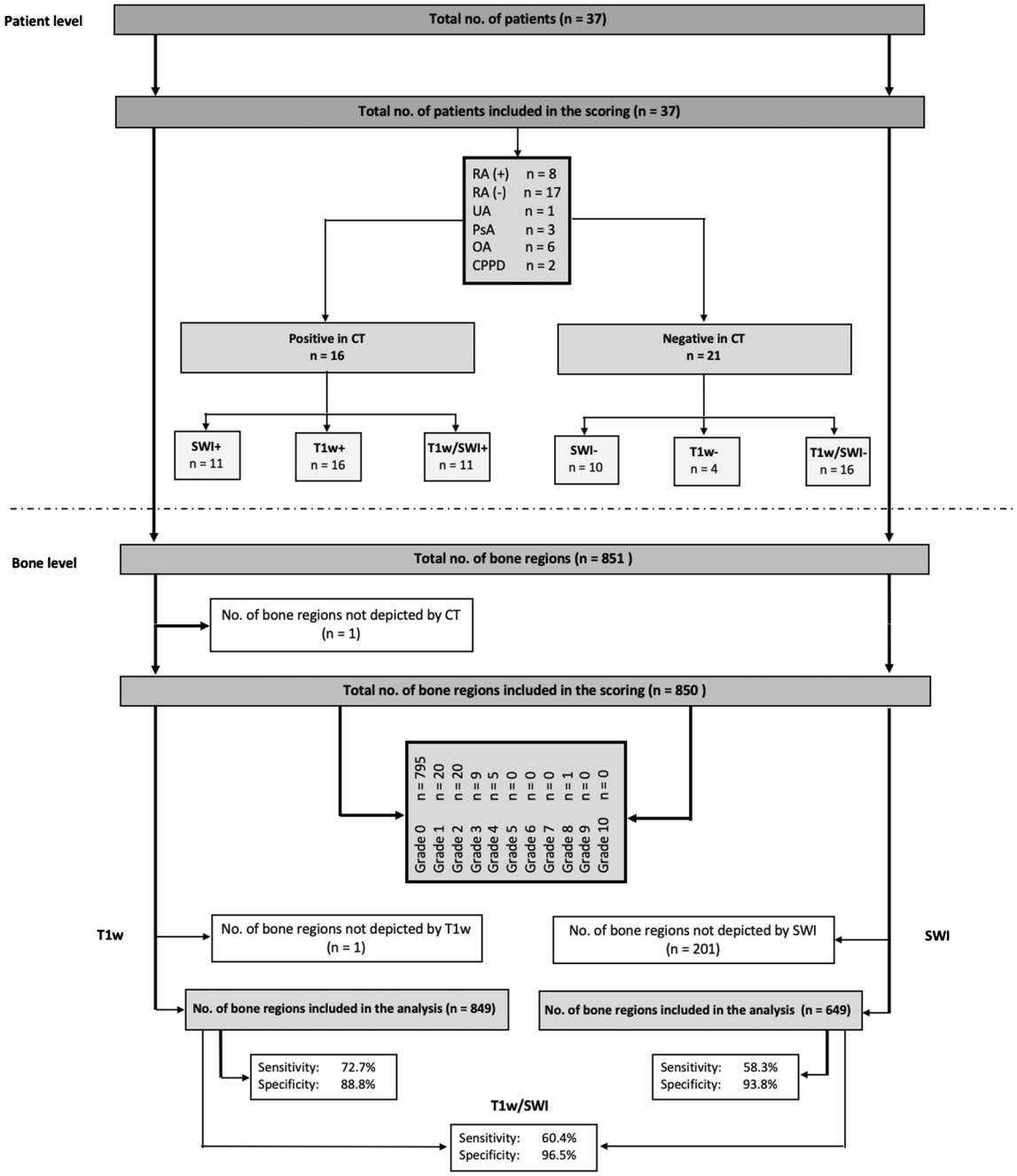

Fig. 1 Study inclusion and scoring results. *n* = number of patients/regions, RA(+) = seropositive rheumatoid arthritis, RA(−) = seronegative rheumatoid arthritis, UA = undifferentiated arthritis, PsA = psoriatic arthritis, OA = osteoarthritis, CPPD = calcium pyrophosphate deposition disease, CT = computed tomography, SWI = Susceptibility-weighted imaging sequence, T1w = T1-weighted imaging sequence. All patients enrolled in the study were included in the scoring. A total of 850 regions were included in the scoring using CT as standard of reference. In SWI, 201 regions were not assessable and therefore were excluded from analysis. In T1w, one region was not detectable. In total, statistical analysis included 649 regions for the comparison of SWI with CT and 849 regions for the comparison of T1w with CT. On the per-bone level, SWI had 93.8% specificity and 58.3% sensitivity compared with 88.8 and 72.7% for T1w. Combined T1w and SWI scoring improved specificity to 96.5%

progression is seen in a patient with inflammatory joint disease, a change in therapy is mandatory. Detection of small erosions in early disease secures the diagnosis and allows differentiation from other joint diseases. Therefore, earlier initiation of anti-inflammatory therapy is possible. On the other hand, imaging has to be highly specific to avoid false-positive findings and overtreatment of healthy people or patients with mechanical differential diagnoses [27]. SWI has the potential to relevantly increase specificity for erosion detection and can thus increase the overall diagnostic accuracy of MRI.

Fig. 2 Examples of imaging findings in study patients. **a** CT; **b** Inverted susceptibility-weighted MRI (SWI); **c** T1-weighted MRI (T1w); 1: 67-year-old man with seropositive rheumatoid arthritis. In CT, erosions were detected i.a. in the head of metacarpal bone II, which was also visible in SWI and T1w (*arrowheads*). CT and SWI detected a bone cyst (without cortical break) in the head of metacarpal bone III. However, on T1w, the cyst was misinterpreted as an erosion in the third metacarpal head (*arrow*). 2: 57-year-old woman with psoriatic arthritis. SWI and T1w showed false-positive detection of an erosion in the base of metacarpal bone V (*arrowheads*). 3: 61-year-old woman with seronegative rheumatoid arthritis. CT and T1w demarcated i.a. an erosion in the head of metacarpal bone III. In SWI, the detection of this erosion was not possible (*arrowheads*)

In our study, the sensitivity of T1w in erosion detection compared to CT was found to be similar to the results of previous studies. In a study of Dohn et al., MRI had 68% sensitivity [28]. While ultrasonography is inexpensive and widely available, it is limited because its diagnostic performance depends on the examiner [29]. A study reported high diagnostic accuracy of ultrasound in detecting synovial tissue activity, while its performance was only moderate in depicting erosive bone changes compared to MRI [30]. In another study of Dohn et al., ultrasonography had 44% sensitivity in small regions of the hand [31]. These findings underline the need for robust imaging modalities to evaluate bone lesions sufficiently.

Table 1 Results of the erosion scoring

Patient level	DA	Sens.	Spec.	PPV	NPV
T1w	0.541	1	0.190	0.484	1
(95% CI)		(0.773–1)	(0.071–0.406)	(0.325–0.648)	(0.454–1)
SWI	0.568	0.688	0.476	0.5	0.667
(95% CI)		(0.442–0.861)	(0.283–0.676)	(0.307–0.693)	(0.415–0.850)
T1w/SWI	0.73	0.688	0.762	0.688	0.762
(95% CI)		(0.442–0.861)	(0.545–0.898)	(0.442–0.861)	(0.545–0.898)
Bone level	DA	Sens.	Spec.	PPV	NPV
T1w	0.878	0.727	0.888	0.31	0.979
(95% CI)		(0.597–0.828)	(0.864–0.908)	(0.237–0.395)	(0.966–0.99)
SWI	0.912	0.583	0.938	0.431	0.966
(95% CI)		(0.443–0.712)	(0.916–0.955)	(0.318–0.552)	(0.947–0.978)
T1w/SWI	0.938	0.604	0.965	0.58	0.968
(95% CI)		(0.463–0.73)	(0.947–0.977)	(0.442–0.706)	(0.951–0.98)
Sum score		Mean	SEM	SD	Pearson's *r*
CT		3.108	1.042	6.341	
T1w		6.595	1.260	7.665	0.761
SWI		2.811	0.740	4.502	0.86
T1w/SWI		2.270	0.752	4.574	0.898

Using CT as standard of reference, specificity and diagnostic accuracy on the patient and bone level was highest for T1w/SWI, followed by SWI. T1w/SWI showed the highest correlation of the sum scores with CT

CT computed tomography, *SWI* susceptibility weighted imaging, *T1w* T1-weighted imaging, *T1w/SWI* combined scoring of SWI and T1w, *DA* diagnostic accuracy, *Sens.* sensitivity, *Spec.* specificity, *PPV* positive predictive value, *NPV* negative predictive value, *95% CI* 95% confidence interval, *SEM* standard error, *SD* standard deviation

SWI is playing an increasing role in the detection of brain hemorrhage in the field of neuroimaging [11] and in the detection of calcification in prostate imaging [32]. Here, paramagnetic and ferromagnetic substances, such as deoxyhemoglobin, hemosiderin, and ferritin, have been shown to cause a positive phase shift of surrounding tissue with a loss of signal in SWI [15, 33, 34]. Previous studies in musculoskeletal imaging show SWI to be highly reliable in detecting calcifications of the tendons and in assessing shoulder spurs [17, 35]. This is attributable to the diamagnetic property of calcium, causing a negative phase shift and hence a high signal.

Some limitations need to be discussed. We included only a small number of patients; however, we were able to derive significant results. In addition, some skeletal regions were

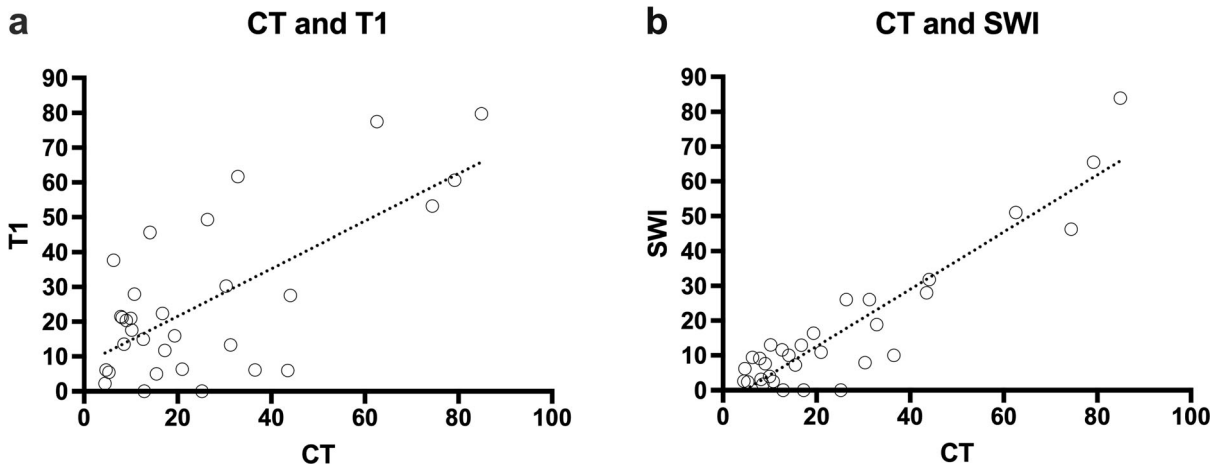

Fig. 3 Correlation of erosion size measurements. The diameter of the surface and depth were measured in millimeters and their product was plotted in the diagram. **a** Correlation of CT with T1w. CT showed a moderate correlation with T1w (Pearson $r = 0.69$, $p < 0.0001$). **b** Correlation of CT with SWI. The diagram presented a high to perfect linear correlation between CT and SWI with a Pearson correlation coefficient of $r = 0.92$ ($p < 0.0001$)

not depicted by SWI due to the small slice number and thickness. However, the sequence can be adapted and optimized for imaging of the hand and finger joints. Further, we used different slice thickness in T1w (3 mm) and SWI (0.8 mm). It needs to be discussed that using the same slice thickness in both sequences could result in a lower difference between T1w and SWI. Due to the longer examination time compared to T1w (5:03 min for SWI and 3:29 min for T1w), SWI is more susceptible to motion artifacts, particularly in assessing the small joints such as the MCP joints. The low sensitivity of SWI for erosion detection can potentially be explained by the relatively strong susceptibility artifacts resulting for tissue intersections between bone, fluid, and tendons in the investigated area. T1w imaging still enables imaging with a higher contrast between bone and surrounding tissue. Further studies with optimized SWI sequence parameters and larger number of study population are needed to assess the added value of SWI in a clinical setting.

In conclusion, SWI has the potential to improve erosion detection in hands by increasing the diagnostic specificity. Compared to T1w, SWI demonstrated a better diagnostic accuracy and may develop into a complementary technique to T1w in the future.

Acknowledgements The authors thank Mrs. Bettina Herwig for language editing.

Compliance with ethical standards

Ethical approval All procedures performed in studies involving human participants were in accordance with the ethical standards of the institutional and/or national research committee and with the 1964 Helsinki Declaration and its later amendments or comparable ethical standards.

Conflict of interest The authors declare that they have no conflicts of interest.

References

1. Brinkmann GH, Norli ES, Bøyesen P, van der Heijde D, Grøvle L, Haugen AJ, et al. Role of erosions typical of rheumatoid arthritis in the 2010 ACR/EULAR rheumatoid arthritis classification criteria: results from a very early arthritis cohort. Ann Rheum Dis. 2017;76(11):1911–4.
2. Knevel R, Lukas C, van der Heijde D, Rincheval N, Combe B, van der Helm-van Mil AH. Defining erosive disease typical of RA in the light of the ACR/EULAR 2010 criteria for rheumatoid arthritis; results of the data driven phase. Ann Rheum Dis. 2013;72(4):590–5.
3. Lee CH, Srikhum W, Burghardt AJ, Virayavanich W, Imboden JB, Link TM, et al. Correlation of structural abnormalities of the wrist and metacarpophalangeal joints evaluated by high-resolution peripheral quantitative computed tomography, 3 Tesla magnetic resonance imaging and conventional radiographs in rheumatoid arthritis. Int J Rheum Dis. 2015;18(6):628–39.
4. Scheel AK, Hermann KG, Ohrndorf S, Werner C, Schirmer C, Detert J, et al. Prospective 7-year follow-up imaging study comparing radiography, ultrasonography, and magnetic resonance imaging in rheumatoid arthritis finger joints. Ann Rheum Dis. 2006;65(5):595–600.
5. Diekhoff T, Hermann KG, Greese J, Schwenke C, Poddubnyy D, Hamm B, et al. Comparison of MRI with radiography for detecting structural lesions of the sacroiliac joint using CT as standard of reference: results from the SIMACT study. Ann Rheum Dis. 2017;76(9):1502–8.
6. Østergaard M, Peterfy CG, Bird P, Gandjbakhch F, Glinatsi D, Eshed I, et al. The OMERACT rheumatoid arthritis magnetic resonance imaging (MRI) scoring system: updated recommendations by the OMERACT MRI in arthritis working group. J Rheumatol. 2017;44(11):1706–12.
7. Chang G, Boone S, Martel D, Rajapakse CS, Hallyburton RS, Valko M, et al. MRI assessment of bone structure and microarchitecture. J Magn Reson Imaging. 2017;46(2):323–37.
8. Shah LM, Hanrahan CJ. MRI of spinal bone marrow: part I, techniques and normal age-related appearances. AJR Am J Roentgenol. 2011;197(6):1298–308.
9. Goldbach-Mansky R, Woodburn J, Yao L, Lipsky PE. Magnetic resonance imaging in the evaluation of bone damage in rheumatoid arthritis: a more precise image or just a more expensive one? Arthritis Rheum. 2003;48(3):585–9.
10. McQueen F, Lassere M, Edmonds J, Conaghan P, Peterfy C, Bird P, et al. OMERACT rheumatoid arthritis magnetic resonance imaging studies. Summary of OMERACT 6 MR imaging module. J Rheumatol. 2003;30(6):1387–92.
11. Wycliffe ND, Choe J, Holshouser B, Oyoyo UE, Haacke EM, Kido DK. Reliability in detection of hemorrhage in acute stroke by a new three-dimensional gradient recalled echo susceptibility-weighted imaging technique compared to computed tomography: a retrospective study. J Magn Reson Imaging. 2004;20(3):372–7.
12. Thomas B, Somasundaram S, Thamburaj K, Kesavadas C, Gupta AK, Bodhey NK, et al. Clinical applications of susceptibility weighted MR imaging of the brain—a pictorial review. Neuroradiology. 2008;50(2):105–16.
13. Haacke EM, Mittal S, Wu Z, Neelavalli J, Cheng YC. Susceptibility-weighted imaging: technical aspects and clinical applications, part 1. AJNR Am J Neuroradiol. 2009;30(1):19–30.
14. Mittal S, Wu Z, Neelavalli J, Haacke EM. Susceptibility-weighted imaging: technical aspects and clinical applications, part 2. AJNR Am J Neuroradiol. 2009;30(2):232–52.
15. Yamada N, Imakita S, Sakuma T, Takamiya M. Intracranial calcification on gradient-echo phase image: depiction of diamagnetic susceptibility. Radiology. 1996;198(1):171–8.
16. Böker SM, Adams LC, Bender YY, Wagner M, Diekhoff T, Fallenberg E, et al. Evaluation of vertebral body fractures using susceptibility-weighted magnetic resonance imaging. Eur Radiol. 2018;28(5):2228–35.
17. Nörenberg D, Armbruster M, Bender YN, Walter T, Ebersberger HU, Diederichs G, et al. Diagnostic performance of susceptibility-weighted magnetic resonance imaging for the assessment of subcoracoacromial spurs causing subacromial impingement syndrome. Eur Radiol. 2017;27(3):1286–94.
18. Wu Z, Mittal S, Kish K, Yu Y, Hu J, Haacke EM. Identification of calcification with MRI using susceptibility-weighted imaging: a case study. J Magn Reson Imaging. 2009;29(1):177–82.
19. Aletaha D, Neogi T, Silman AJ, Funovits J, Felson DT, Bingham CO 3rd, et al. 2010 rheumatoid arthritis classification criteria: an American College of Rheumatology/European League Against Rheumatism Collaborative Initiative. Ann Rheum Dis. 2010;69(9):1580–8.
20. Østergaard M, Edmonds J, McQueen F, Peterfy C, Lassere M, Ejbjerg B, et al. An introduction to the EULAR-OMERACT rheumatoid arthritis MRI reference image atlas. Ann Rheum Dis. 2005;64(Suppl 1):i3–7.

21. Tan YK, Conaghan PG. Imaging in rheumatoid arthritis. Best Pract Res Clin Rheumatol. 2011;25(4):569–84.
22. Lee DM, Weinblatt ME. Rheumatoid arthritis. Lancet. 2001;358(9285):903–11.
23. Aletaha D, Smolen J, Ward MM. Measuring function in rheumatoid arthritis: identifying reversible and irreversible components. Arthritis Rheum. 2006;54(9):2784–92.
24. Baum R, Gravallese EM. Bone as a target organ in rheumatic disease: impact on osteoclasts and osteoblasts. Clin Rev Allergy Immunol. 2016;51(1):1–15.
25. Heinlen L, Humphrey MB. Skeletal complications of rheumatoid arthritis. Osteoporos Int. 2017;28(10):2801–12.
26. McQueen FM, Stewart N, Crabbe J, Robinson E, Yeoman S, Tan PL, et al. Magnetic resonance imaging of the wrist in early rheumatoid arthritis reveals progression of erosions despite clinical improvement. Ann Rheum Dis. 1999;58(3):156–63.
27. Husberg M, Bernfort L, Hallert E. Costs and disease activity in early rheumatoid arthritis in 1996-2000 and 2006-2011, improved outcome and shift in distribution of costs: a two-year follow-up. Scand J Rheumatol. 2018;47(5):378–383.
28. Døhn UM, Ejbjerg BJ, Court-Payen M, Hasselquist M, Narvestad E, Szkudlarek M, et al. Are bone erosions detected by magnetic resonance imaging and ultrasonography true erosions? A comparison with computed tomography in rheumatoid arthritis metacarpophalangeal joints. Arthritis Res Ther. 2006;8(4):R110.
29. Hoving JL, Buchbinder R, Hall S, Lawler G, Coombs P, McNealy S, et al. A comparison of magnetic resonance imaging, sonography, and radiography of the hand in patients with early rheumatoid arthritis. J Rheumatol. 2004;31(4):663–75.
30. Saran S, Bagarhatta M, Saigal R. Diagnostic accuracy of ultrasonography in detection of destructive changes in small joints of hands in patients of rheumatoid arthritis: a comparison with magnetic resonance imaging. J Assoc Physicians India. 2016;64(11):26–30.
31. Døhn UM, Terslev L, Szkudlarek M, Hansen MS, Hetland ML, Hansen A, et al. Detection, scoring and volume assessment of bone erosions by ultrasonography in rheumatoid arthritis: comparison with CT. Ann Rheum Dis. 2013;72(4):530–4.
32. Bai Y, Wang MY, Han YH, Dou SW, Lin Q, Guo Y, et al. Susceptibility weighted imaging: a new tool in the diagnosis of prostate cancer and detection of prostatic calcification. PLoS One. 2013;8(1):e53237.
33. Zhu WZ, Qi JP, Zhan CJ, Shu HG, Zhang L, Wang CY, et al. Magnetic resonance susceptibility weighted imaging in detecting intracranial calcification and hemorrhage. Chin Med J. 2008;121(20):2021–5.
34. Gupta RK, Rao SB, Jain R, Pal L, Kumar R, Venkatesh SK, et al. Differentiation of calcification from chronic hemorrhage with corrected gradient echo phase imaging. J Comput Assist Tomogr. 2001;25(5):698–704.
35. Nörenberg D, Ebersberger HU, Walter T, Ockert B, Knobloch G, Diederichs G, et al. Diagnosis of calcific tendonitis of the rotator cuff by using susceptibility-weighted MR imaging. Radiology. 2016;278(2):475–84.